Research Square

Preprints are preliminary reports that have not undergone peer review.
They should not be considered conclusive, used to inform clinical practice,
or referenced by the media as validated information.

Elastic-Contrast Screening and Validation Roadmap for Refractory High-Entropy Alloy/Intermetallic Heterostructures

Hafid Aourag

h.aourag@mesrs.dz

USTO

Research Article

Keywords: Refractory high-entropy alloys, Intermetallic compounds, Heterostructures, Elastic-contrast screening, Design-space prioritisation, Interface validation, DFT, High-temperature materials

Posted Date: September 30th, 2026

DOI: https://doi.org/10.21203/rs.3.rs-10984263/v1

License: This work is licensed under a Creative Commons Attribution 4.0 International License.
Read Full License

Additional Declarations: No competing interests reported.

Elastic-Contrast Screening and Validation Roadmap for Refractory High-Entropy Alloy/Intermetallic Heterostructures

Hafid Aourag (Corresponding author)

Physics Department, University of Science and Technology of Oran Mohamed Boudiaf (USTO-MB), Oran 31000, Algeria

Email corresponding author! h.aourag@mesrs.dz

Abstract

Coatings and structural materials intended for service at 1000–1500 °C must simultaneously retain mechanical strength, phase stability, oxidation resistance, and interfacial integrity. This work presents a physics-informed design-space prioritisation framework for refractory high-entropy alloy (RHEA)/intermetallic heterostructures. The purpose is not to identify a universally optimal architecture from elastic contrast alone, but to transparently prioritise candidate layer pairs for focused thermodynamic, interfacial, temperature-dependent mechanical, and experimental validation. DFT-derived elastic properties for BCC RHEA special-quasirandom-structure approximants are combined with room-temperature elastic descriptors for B2 NiAl, $L1_2$ Ni_3Al, and $D0_{22}$ $TiAl_3$. For cubic NiAl and Ni_3Al, polycrystalline descriptors are derived by Voigt–Reuss–Hill averaging of reported single-crystal stiffness constants, yielding $E_{VRH} = 183.6$ GPa and 199.8 GPa, respectively. $TiAl_3$ is defined as the equilibrium tetragonal $D0_{22}$ reference phase; its previously compiled $E = 183.0$ GPa input is retained as a phase-specific room-temperature screening descriptor. A Young's-modulus mismatch index, k_E, is used as a first-pass descriptor of elastic contrast relevant to Koehler-type interface-strengthening concepts; it is not treated as a direct prediction of multilayer hardness, interface strength, or high-temperature service performance. Within the primary reference set, Cr–Mo–W–Re/$D0_{22}$-$TiAl_3$ exhibits the largest present k_E value, 0.333, closely followed by Cr–Mo–W–Re/B2-NiAl, 0.331. Ta–Mo–W–Re/B2-NiAl, with $k_E = 0.302$, is retained as a technologically established B2 benchmark. Al_3Zr_5-containing pairs are excluded from the quantitative ranking and retained only as separate high-risk/high-reward prospective hypotheses. The framework distinguishes elastic screening from final performance prediction and defines a validation sequence covering phase stability, reaction thermodynamics, diffusion kinetics, interface structure and adhesion, thermal-expansion compatibility, oxidation behaviour, and thermomechanical response.

Keywords: Refractory high-entropy alloys; Intermetallic compounds; Heterostructures; Elastic-contrast screening; Design-space prioritisation; Interface validation; DFT; High-temperature materials

1 Introduction

The development of materials for extreme thermal and mechanical environments remains a major challenge in materials engineering. Hypersonic systems, rocket-nozzle components, gas-turbine hardware, and advanced nuclear-energy systems may require structural or protective materials that operate above 1000 °C while retaining mechanical integrity and resistance to oxidation and thermal cycling [1,2]. Refractory high-entropy alloys (RHEAs) are promising candidates because they combine high concentrations of refractory elements with potentially high melting-temperature descriptors, solid-solution strengthening, and retention of useful mechanical properties at elevated temperature [3–5]. WReTaMo, for example, has been reported to retain measurable compressive strength at 1600 °C [6].

Ordered intermetallic compounds may provide complementary properties in layered or graded architectures. B2 NiAl, $L1_2$ Ni_3Al, and $D0_{22}$ $TiAl_3$ possess technologically relevant combinations of stiffness, strength, oxidation behaviour, and ordered crystal structures [7–10]. Their practical response depends on composition, crystal structure, microstructure, orientation, temperature, and environment. Their use as reference layers in a RHEA/intermetallic heterostructure therefore does not imply interface stability or equivalent behaviour after coupling to a refractory alloy.

Alternating layers of elastically dissimilar materials can alter dislocation motion, stress partitioning, and residual-stress development. Koehler's modulus-mismatch concept provides a classical basis for considering elastic contrast in multilayered materials [11]. In real heterostructures, strengthening also depends on shear-modulus mismatch, elastic anisotropy, orientation relationships, interface coherency, layer thickness, defect structure, and temperature-dependent plasticity [12–14]. Elastic contrast alone is insufficient to predict hardness, interface strength, or service performance.

Systematic screening of RHEA/intermetallic combinations is limited by the breadth of the compositional design space and incomplete availability of phase-consistent elastic, thermodynamic, kinetic, and environmental data. Rather than claiming that a particular RHEA/intermetallic pair is intrinsically optimal, the present work is a design-space prioritisation study. It applies a transparent, physics-informed first-pass screening procedure to identify architectures that merit priority in subsequent calculations and experiments. The principal contribution is a transferable decision framework for prioritising candidate heterostructures, rather than the identification of a single optimal composition.

2 Materials and Methods

2.1 RHEA dataset and DFT methodology

The RHEA dataset comprises BCC quaternary, quinary, and senary alloy approximants containing Ta, Mo, W, Re, V, Nb, Cr, Ti, and Hf. DFT-derived elastic properties for BCC RHEA approximants were paired with room-temperature elastic descriptors for selected ordered intermetallic reference phases. Rule-of-mixtures melting-temperature values are used only as comparative refractory-character indicators; they do not represent alloy liquidus temperatures, solidus temperatures, phase-transformation temperatures, or thermodynamic stability limits.

DFT calculations were performed using the Vienna *Ab initio* Simulation Package (VASP), the projector-augmented-wave method, and the Perdew–Burke–Ernzerhof generalised-gradient approximation [15–17]. Chemical disorder was represented by 128-atom special quasirandom structures reproducing pair correlations through the third-neighbour shell [18]. Three independent SQS realisations were evaluated per composition. A 500 eV plane-wave cutoff, reciprocal-space spacing no greater than 0.025 $Å^{-1}$, electronic convergence of 10^{-6} eV per supercell, Methfessel–Paxton smearing of 0.2 eV, and force convergence below 0.01 eV $Å^{-1}$ were used. Elastic stiffness matrices were obtained by a stress–strain approach with six independent deformation modes and strain amplitudes of ±0.5% and ±1.0%. Mechanical stability of reduced-symmetry SQS cells was assessed by positive definiteness of the full stiffness matrix. Polycrystalline moduli were obtained by Voigt–Reuss–Hill averaging [19]. Spin-polarised calculations were used for Cr-containing systems.

The final supplementary archive should include POSCAR/CIF structures, input settings, complete stiffness matrices, calculated elastic moduli, and standard deviations across the three SQS realisations.

2.2 Intermetallic references

The primary quantitative ranking includes stoichiometric B2 NiAl, $L1_2$ Ni_3Al, and $D0_{22}$ $TiAl_3$. All values are room-temperature screening descriptors and do not represent complete temperature- or orientation-dependent elastic response.

B2 NiAl. Stoichiometric Ni–50Al, $Pm\bar{3}m$, was selected as the reference state. The adopted room-temperature stiffness constants are $C_{11} = 211.5$ GPa, $C_{12} = 143.2$ GPa, and $C_{44} = 112.1$ GPa. VRH averaging gives $B = 166.0$ GPa, $G_{VRH} = 69.8$ GPa, $E_{VRH} = 183.6$ GPa, and $\nu = 0.316$. B2 NiAl has a measurable homogeneity range; off-stoichiometry modifies sublattice defect populations, stiffness constants, and elastic anisotropy. Fixing stoichiometric Ni–50Al avoids mixing composition-dependent elastic data [20,21].

$L1_2$ Ni_3Al. Ordered γ′-Ni_3Al, $Pm\bar{3}m$, was selected as the reference state. The adopted room-temperature stiffness constants are $C_{11} = 223.5$ GPa, $C_{12} = 149.0$ GPa, and $C_{44} = 122.9$ GPa. VRH averaging gives $B = 173.8$ GPa, $G_{VRH} = 76.3$ GPa, $E_{VRH} = 199.8$ GPa, and $\nu = 0.308$. The data are used only as defined room-

temperature reference inputs because the elastic response is composition and temperature dependent [22,23].

$D0_{22}$ $TiAl_3$. $TiAl_3$ is explicitly defined as the equilibrium tetragonal $D0_{22}$ reference phase. The present first-pass screening retains the phase-specific input $E = 183.0$ GPa at 298 K. The final supplementary dataset must identify the exact source table/page and give the selected $D0_{22}$ lattice parameters, full stiffness tensor $C_{11}, C_{12}, C_{13}, C_{33}, C_{44}, C_{66}$, and resulting tetragonal VRH values when available. Until a homogeneous DFT calculation is performed, this input is used transparently as a phase-specific compiled descriptor, not as a universal $TiAl_3$ property [24].

Al_3Zr_5 prospective hypothesis. Al_3Zr_5 is excluded from the quantitative ranking. Its phase-specific identity, elastic tensor, stability, oxidation behaviour, and compatibility with Ta-, Mo-, W-, Re-, and Cr-containing RHEAs require independent validation. It is retained only as a high-risk/high-reward future research hypothesis.

2.3 Elastic-contrast screening

The room-temperature Young's-modulus mismatch descriptor is:

$$k_E = \frac{|E_{HEA} - E_{IMC}|}{E_{HEA} + E_{IMC}}.$$

The quantity k_E is used as a first-pass descriptor of elastic incompatibility relevant to Koehler-type interface-strengthening concepts. It is not a direct Koehler coefficient. A complete interface-strengthening analysis must include temperature-dependent shear-modulus mismatch, elastic anisotropy, interface coherency, orientation relationships, layer thickness, interface structure, and dislocation/interface interactions. Large elastic contrast can nevertheless affect stress partitioning and residual-stress development during thermal cycling and mechanical loading. Thus, k_E is used as a conservative boundary-condition filter before higher-fidelity calculations are undertaken.

For cubic phases:

$$B = \frac{C_{11} + 2C_{12}}{3}, G_V = \frac{C_{11} - C_{12} + 3C_{44}}{5},$$

$$G_R = \frac{5(C_{11} - C_{12})C_{44}}{4C_{44} + 3(C_{11} - C_{12})}, G_{VRH} = \frac{G_V + G_R}{2},$$

$$E_{VRH} = \frac{9BG_{VRH}}{3B + G_{VRH}}, \nu = \frac{3B - 2G_{VRH}}{2(3B + G_{VRH})}.$$

When phase-consistent shear moduli are available, the shear mismatch may be reported as:

$$k_G = \frac{|G_{HEA} - G_{IMC}|}{G_{HEA} + G_{IMC}}.$$

2.4 Multi-criteria validation framework

A normalised multi-criteria index is proposed for later validation stages:

$$\Phi = w_1\tilde{T}_{stab} + w_2 S_{reaction} + w_3\tilde{k}_E + w_4\tilde{S}_{ox} + w_5 S_{CTE} + w_6\widetilde{H}_{IMC} + w_7\widetilde{D}_{HEA}.$$

The terms represent high-temperature phase stability, interfacial reaction resistance, elastic contrast, oxidation resistance, thermal-expansion compatibility, intermetallic strength, and RHEA ductility/toughness. No definitive ranking by Φ is claimed because homogeneous datasets are not available for every descriptor. Ta–Mo–W–Re/B2-NiAl is retained as a technological benchmark because it combines substantial contrast with an established B2 reference; this does not imply proven chemical compatibility with the RHEA.

2.5 Validation roadmap

The framework prioritises candidates for the following validation sequence:

1. Thermodynamic viability: convex-hull stability, reaction driving forces, competing phases, and chemical-potential windows.
2. Kinetic persistence: diffusion coefficients, migration barriers, and finite-time thermal exposure.
3. Structural compatibility: orientation relationships, lattice mismatch, residual strain, interface energy, and termination.
4. Mechanical viability: $k_G(T)$, anisotropic elastic response, ideal interface shear strength, work of adhesion, and dislocation/interface interactions.
5. Environmental viability: oxidation products, oxide-scale adhesion, cyclic thermal stresses, and atmospheric compatibility.
6. Experimental validation: deposition, annealing, thermal cycling, microstructural characterisation, and mechanical testing.

3 Results

3.1 Elastic data and primary ranking

The results are interpreted as a prioritisation of candidate architectures, not as a final optimisation of high-temperature performance. Al_3Zr_5-containing pairs are excluded from the principal ranking. NiAl and Ni_3Al use VRH-derived room-temperature moduli of 183.6 and 199.8 GPa, respectively. $D0_{22}$ $TiAl_3$ uses the retained phase-specific screening input of 183.0 GPa.

Within the B2-NiAl/$L1_2$-Ni_3Al/$D0_{22}$-$TiAl_3$ reference set, Cr–Mo–W–Re/$D0_{22}$-$TiAl_3$ has the largest present mismatch index, $k_E = 0.333$, followed by Cr–Mo–W–Re/B2-NiAl, $k_E = 0.331$. Ta–Mo–W–Re/$D0_{22}$-$TiAl_3$ and Ta–Mo–W–Re/B2-NiAl have $k_E = 0.304$ and 0.302, respectively. Ta–Mo–W–Re/B2-NiAl combines substantial elastic contrast with $T_m = 3335$ K and a bulk-HEA B/G value of 2.19, and is therefore retained as the technological B2 benchmark. The elastic properties and room-temperature Young's-modulus mismatch indices of the primary RHEA/intermetallic reference candidates are compiled in Table 1.

Table 1. Primary RHEA/intermetallic reference candidates ranked by the room-temperature Young's-modulus mismatch index, k_E.

Rank	RHEA layer	Intermetallic layer	E_{HEA} (GPa)	E_{IMC} (GPa)	k_E	B/G of RHEA	T_m (K)	Candidate role
1	Cr–Mo–W–Re	$D0_{22}$-$TiAl_3$	365.6	183.0	0.333	1.94	3058	Highest elastic-contrast reference hypothesis
2	Cr–Mo–W–Re	B2-NiAl	365.6	183.6	0.331	1.94	3058	Alternative B2 reference
3	Ta–Mo–W–Re	$D0_{22}$-$TiAl_3$	342.6	183.0	0.304	2.19	3335	Alternative Ti-aluminide hypothesis
4	Ta–Mo–W–Re	B2-NiAl	342.6	183.6	0.302	2.19	3335	Technological B2 benchmark
5	Ta–Mo–W–Re	$L1_2$-Ni_3Al	342.6	199.8	0.263	2.19	3335	Alternative $L1_2$ hypothesis
6	Nb–Ta–Mo–W–Re	B2-NiAl	297.1	183.6	0.236	2.34	3218	Balanced quinary B2 reference

*Note: (k_E=	E_{HEA}-E_{IMC}	/(E_{HEA}+E_{IMC})). NiAl and Ni_3Al values are room-temperature VRH moduli derived from reported cubic stiffness constants. $D0_{22}$-$TiAl_3$ uses a phase-specific compiled reference input. T_m is a rule-of-mixtures refractory-character descriptor and is not an equilibrium liquidus or phase-stability metric. Al_3Zr_5-containing candidates are intentionally excluded from the principal quantitative ranking.*

The complete ranking of the primary RHEA/intermetallic reference heterostructures based on the Young's-modulus mismatch index is presented in Fig. 1. The figure visualises the relative elastic contrast among the shortlisted systems and should be interpreted only as a first-pass screening result, not as a prediction of interfacial strength, phase stability, or high-temperature service performance.

3.2 Candidate roles

- **Highest-elastic-contrast reference hypothesis:** Cr–Mo–W–Re/$D0_{22}$-$TiAl_3$.
- **Technological benchmark:** Ta–Mo–W–Re/B2-NiAl.
- **Alternative design hypotheses:** Cr–Mo–W–Re/B2-NiAl, Ta–Mo–W–Re/$D0_{22}$-$TiAl_3$, Ta–Mo–W–Re/$L1_2$-Ni_3Al, and Nb–Ta–Mo–W–Re/B2-NiAl.
- **Separate prospective hypothesis:** Al_3Zr_5-containing pairs, excluded from quantitative comparison.

3.3 Two-descriptor comparison

Figure 2 compares k_E with the rule-of-mixtures melting-temperature descriptor T_m. The map illustrates a trade-off between elastic contrast and comparative refractory character; it does not establish phase stability, liquidus temperature, reaction resistance, oxidation resistance, or service performance. Ta–Mo–W–Re/B2-NiAl combines $k_E = 0.302$ with $T_m = 3335$ K, making it a useful benchmark for subsequent validation.

4 Discussion

4.1 Scope of the ranking

The ranking does not establish a universally optimal high-temperature heterostructure. It identifies regions of the RHEA/intermetallic design space that combine substantial room-temperature elastic contrast with comparative refractory character. Cr–Mo–W–Re/$D0_{22}$-$TiAl_3$ is the highest-elastic-contrast candidate in the defined primary reference set, whereas Ta–Mo–W–Re/B2-NiAl serves a complementary role as a technological benchmark.

A high k_E does not guarantee low interface energy, high work of adhesion, coherent epitaxy, reaction resistance, oxidation protection, or damage tolerance. NiAl is technologically relevant because of its established B2 character, but its compatibility with a specific RHEA must be calculated and measured rather than assumed. Prior studies on refractory solute effects at Ni/Ni_3Al and γ/γ′ interfaces provide context but do not establish stability of the exact RHEA/intermetallic interfaces considered here [25,26].

4.2 NiAl composition dependence

B2 NiAl has a measurable homogeneity range. Off-stoichiometry changes defect populations on the Ni and Al sublattices and affects C_{11}, C_{12}, C_{44}, $C' = (C_{11} - C_{12})/2$, and the Zener anisotropy ratio $A = 2C_{44}/(C_{11} - C_{12})$. The use of stoichiometric Ni–50Al and a stated stiffness dataset avoids mixing composition-dependent elastic inputs. The derived VRH modulus remains a room-temperature screening descriptor, not a representation of the full composition–temperature response of practical NiAl-based alloys [20,21].

4.3 Al_3Zr_5 prospective hypothesis

Al_3Zr_5-containing pairs are retained only as prospective high-risk/high-reward hypotheses. Their potential large contrast relative to high-modulus RHEAs motivates future investigation but does not justify quantitative ranking. Future inclusion requires validated phase identity, elastic constants and VRH moduli at a stated temperature, convex-hull and finite-temperature stability analysis, reaction screening against the RHEA, diffusion calculations, interface-energy and work-of-adhesion calculations, and evaluation of oxidation and thermal-expansion compatibility.

4.4 Interface-centred validation

For a periodic DFT interface supercell containing two equivalent interfaces, the interface energy can be written as:

$$\gamma_{int} = \frac{E_{RHEA/IMC} - E^{ref}_{RHEA} - E^{ref}_{IMC}}{2A}.$$

The work of adhesion is:

$$W_{ad} = \gamma_{RHEA}^{surf} + \gamma_{IMC}^{surf} - \gamma_{int}.$$

For non-stoichiometric terminations, interface excess free energy should be formulated as a function of chemical potentials constrained by parent and competing phases [27]. These calculations are required because interface preference cannot be inferred from elastic mismatch alone.

4.5 Decision framework and validation roadmap

The criteria, symbols, and operational definitions proposed for the later multi-criteria validation stage are summarised in Table 2. These descriptors are intended to guide subsequent assessment after the initial elastic-contrast screening; they do not constitute a final quantitative performance ranking in the present work.77

Table 2. Terms of the multi-criteria decision framework.

Criterion	Symbol	Description
High-temperature phase stability	$\tilde{T}_{stab}$	Normalised fraction of intended phases retained at the defined temperature and environment
Interfacial reaction resistance	$S_{reaction}$	Resistance to interfacial reaction based on reaction thermodynamics and kinetics
Elastic contrast	$\tilde{k}_E$	Normalised Young's-modulus mismatch descriptor
Oxidation resistance	$\tilde{S}_{ox}$	Normalised oxidation-resistance score
Thermal-expansion compatibility	S_{CTE}	Score penalising thermal-expansion mismatch and cyclic thermal stress
Intermetallic strength	$\tilde{H}_{IMC}$	Normalised elevated-temperature hardness or strength descriptor
RHEA ductility/toughness	$\tilde{D}_{HEA}$	Normalised ductility or fracture-related descriptor

The overall sequence linking first-pass elastic screening to thermodynamic, interfacial, kinetic, environmental, and experimental validation is summarised in Fig. 3. This roadmap is intended to guide the progressive evaluation of candidate RHEA/intermetallic heterostructures beyond the initial elastic-contrast descriptor.

5 Conclusions

This work establishes an elastic-contrast screening and validation roadmap for RHEA/intermetallic heterostructures for high-temperature applications. Its principal contribution is not a deterministic

prediction of a single optimal pair, but a transparent and reproducible decision baseline that reduces a broad design space to high-value candidates for targeted computation and experiment.

Within the primary reference set, Cr–Mo–W–Re/D0_{22}-$TiAl_3$ has the largest present Young's-modulus mismatch index, $k_E = 0.333$, closely followed by Cr–Mo–W–Re/B2-NiAl, $k_E = 0.331$. Ta–Mo–W–Re/B2-NiAl is retained as the technological B2 benchmark because it combines substantial elastic contrast, a high estimated rule-of-mixtures melting-temperature descriptor, and an established intermetallic reference for comparative interface-centred work. These outcomes are prioritisation results, not validated high-temperature material solutions.

Although Koehler-type strengthening depends more directly on shear-modulus mismatch, elastic anisotropy, interface structure, and dislocation/interface interactions, k_E provides a practical first-pass measure of elastic incompatibility. Large elastic contrast can influence stress partitioning and residual-stress development during thermal and mechanical loading. Accordingly, k_E is used as a conservative screening descriptor rather than as a direct strengthening or service-performance predictor.

Al_3Zr_5-containing pairs are deliberately excluded from the principal ranking and retained only as prospective high-risk/high-reward hypotheses. Their potential contrast motivates further research, but no comparative performance or feasibility claim is made until their phase identity, elastic properties, stability, reaction chemistry, diffusion, interface structure, and environmental durability are independently established.

The final selection of viable high-temperature heterostructures must combine temperature-dependent shear-modulus contrast, phase stability, reaction driving force, diffusion kinetics, interface orientation and coherency, work of adhesion, thermal-expansion compatibility, oxidation resistance, and thermomechanical fracture response. The roadmap therefore avoids blind combinatorial searches and defines the sequence required to transform first-pass elastic-screening hypotheses into validated heterostructure designs.

Data availability

The datasets generated and analysed during the current study are provided in the Supplementary Information. Supplementary Dataset S1 contains the RHEA elastic-property dataset, SQS-realisation statistics, intermetallic elastic-data provenance, VRH calculations, and the complete k_E ranking. Supplementary Code S1 contains the script used for VRH averaging, mismatch-index calculations, and figure generation.

Funding

The author received no specific funding for this work. [Replace this statement if funding was received.]

Author contributions

Hafid Aourag conceived the study, developed the methodology, performed the calculations and data analysis, prepared the figures, wrote the original draft, and revised the manuscript.

Competing interests

The author declares no competing interests.

AI Uses

During the preparation of this work, the author used Perplexity to improve the language and readability of the manuscript. After using this tool/service, the author reviewed and edited the content as needed and takes full responsibility for the content of the publication.

Supplementary Table S1

Elastic-data provenance and VRH treatment.

Phase	Defined reference state	Temperature	Single-crystal elastic input	Derived/used descriptor	Method	Primary source
NiAl	B2 Ni–50Al, $Pm\bar{3}m$	~300 K	$C_{11} = 211.5$, $C_{12} = 143.2$, $C_{44} = 112.1$ GPa	$B = 166.0$, $G_{VRH} = 69.8$, $E_{VRH} = 183.6$ GPa, $\nu = 0.316$	Cubic VRH	Rusović and Warlimont [20,21]
Ni_3Al	$L1_2$ Ni_3Al, $Pm\bar{3}m$	~300 K	$C_{11} = 223.5$, $C_{12} = 149.0$, $C_{44} = 122.9$ GPa	$B = 173.8$, $G_{VRH} = 76.3$, $E_{VRH} = 199.8$ GPa, $\nu = 0.308$	Cubic VRH	Frankel et al. [22]; Prikhodko et al. [23]
$TiAl_3$	$D0_{22}$ tetragonal reference	298 K	Complete $D0_{22}$ tensor to be supplied in final SI	$E = 183.0$ GPa	Phase-specific compiled input	Ti–Al first-principles study [24]
Al_3Zr_5	Prospective only	Not ranked	Not used in primary ranking	Previously compiled $E = 143.4$ GPa not used quantitatively	Excluded	Independent phase-specific validation required

References

[1] P.H. Mayrhofer, C. Mitterer, L. Hultman, H. Clemens, Prog. Mater. Sci. 51 (2006) 1032–1114.

[2] S. Vepřek, M.G.J. Vepřek-Heijman, Surf. Coat. Technol. 202 (2008) 5063–5073.

[3] D.B. Miracle, O.N. Senkov, Acta Mater. 122 (2017) 448–511.

[4] O.N. Senkov, G.B. Wilks, D.B. Miracle, C.P. Chuang, P.K. Liaw, Intermetallics 18 (2010) 1758–1765.

[5] O.N. Senkov, J.D. Miller, D.B. Miracle, C. Woodward, Nat. Commun. 6 (2015) 6529.

[6] Y.X. Wan, Q.Q. Wang, J.Y. Mo, Z.B. Zhang, X. Wang, X.B. Liang, B.L. Shen, Adv. Eng. Mater. 24 (2022) 2100765.

[7] R. Darolia, JOM 43 (1991) 44–49.

[8] D.B. Miracle, Acta Metall. Mater. 41 (1993) 649–684.

[9] Y.-W. Kim, JOM 47 (1995) 38–42.

[10] S.C. Deevi, V.K. Sikka, Intermetallics 4 (1996) 357–375.

[11] J.S. Koehler, Phys. Rev. B 2 (1970) 547–551.

[12] P.M. Anderson, C. Li, Nanostruct. Mater. 5 (1995) 349–362.

[13] A. Misra, J.P. Hirth, R.G. Hoagland, Acta Mater. 53 (2005) 4817–4826.

[14] R.G. Hoagland, J.P. Hirth, A. Misra, Philos. Mag. 86 (2006) 3537–3558.

[15] G. Kresse, J. Furthmüller, Phys. Rev. B 54 (1996) 11169–11186.

[16] P.E. Blöchl, Phys. Rev. B 50 (1994) 17953–17979.

[17] J.P. Perdew, K. Burke, M. Ernzerhof, Phys. Rev. Lett. 77 (1996) 3865–3868.

[18] A. Zunger, S.-H. Wei, L.G. Ferreira, J.E. Bernard, Phys. Rev. Lett. 65 (1990) 353–356.

[19] R. Hill, Proc. Phys. Soc. A 65 (1952) 349–354.

[20] N. Rusović, H. Warlimont, The elastic behaviour of B2-NiAl, Phys. Status Solidi A 44 (1977) 609–619. https://doi.org/10.1002/pssa.2210440225.

[21] N. Rusović, H. Warlimont, Young's modulus of B2-NiAl alloys, Phys. Status Solidi A 53 (1979) 283–288. https://doi.org/10.1002/pssa.2210530132.

[22] J. Frankel, J.C. Jamieson, J. Vassiliou, D.P. Dandekar, W. Scholz, The Elastic Constants of Ni_3Al to 1.4 GPa, ARCCB-TR-86018, 1986.

[23] S.V. Prikhodko, H. Yang, A.J. Ardell, J.D. Carnes, D.G. Isaak, Temperature and composition dependence of the elastic constants of Ni_3Al, Metall. Mater. Trans. A 30 (1999) 2403–2408. https://doi.org/10.1007/s11661-999-0248-9.

[24] First-principles study on mechanical properties and electronic structures of Ti–Al intermetallic compounds, J. Mater. Res. 34 (2019) 1112–1120. https://doi.org/10.1557/jmr.2018.494.

[25] Y. Lu, Y. Zhang, H. Chen, L. Zhang, J. Appl. Phys. 128 (2020) 175307.

[26] J. Wang, Y. Lu, S. Wang, J. Mater. Sci. 55 (2020) 13400–13415.

[27] J. Rogal, R. Drautz, Ab initio thermodynamics of interfaces, in: M. Hÿtch, P. Nellist (Eds.), Advances in Imaging and Electron Physics, Vol. 183, Elsevier, 2014.

Figures Captions

Fig. 1. Primary Young's-modulus-mismatch ranking for RHEA/intermetallic reference heterostructures. The mismatch index is $k_E = |E_{HEA} - E_{IMC}|/(E_{HEA} + E_{IMC})$. NiAl and Ni_3Al values are room-temperature VRH moduli calculated from reported cubic stiffness constants; $D0_{22}$-$TiAl_3$ uses the phase-specific compiled reference input. The graph is a relative elastic-contrast screening result and does not predict Koehler strengthening, interfacial strength, multilayer hardness, phase stability, or high-temperature service performance. Al_3Zr_5-containing systems are excluded pending phase-specific validation.

Fig. 2. Elastic contrast versus comparative refractory character for the primary reference candidates. k_E is plotted against the rule-of-mixtures melting-temperature descriptor T_m. Ta–Mo–W–Re/B2-NiAl combines $k_E = 0.302$ with $T_m = 3335$ K. The map is not a phase-stability, liquidus-temperature, or service-performance diagram.

Fig. 3. Elastic-contrast screening and validation roadmap for RHEA/intermetallic heterostructures. The workflow progresses from candidate-space definition and first-pass screening using k_E and, where

available, k_G, through thermodynamic phase stability, interface chemistry and adhesion, diffusion, environmental stability, and experimental validation.

Figures

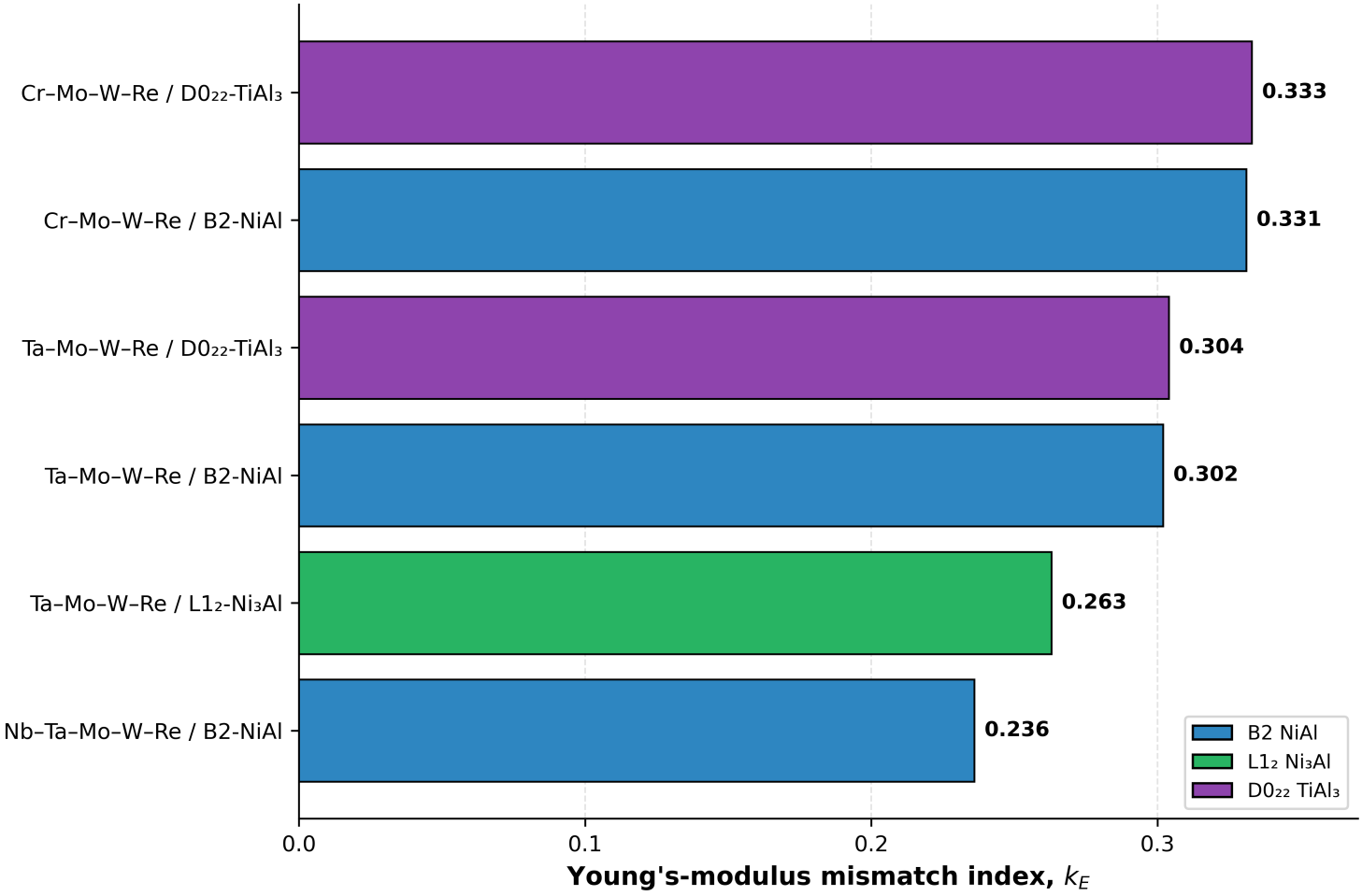


Figure 1

Primary Young's-modulus-mismatch ranking for RHEA/intermetallic reference heterostructures. The mismatch index is $k_E=|E_{HEA}-E_{IMC}|/(E_{HEA}+E_{IMC})$. NiAl and Ni_3Al values are room-temperature VRH moduli calculated from reported cubic stiffness constants; $D0_{22}$-$TiAl_3$ uses the phase-specific compiled reference input. The graph is a relative elastic-contrast screening result and does not predict Koehler strengthening, interfacial strength, multilayer hardness, phase stability, or high-temperature service performance. Al_3Zr_5-containing systems are excluded pending phase-specific validation.

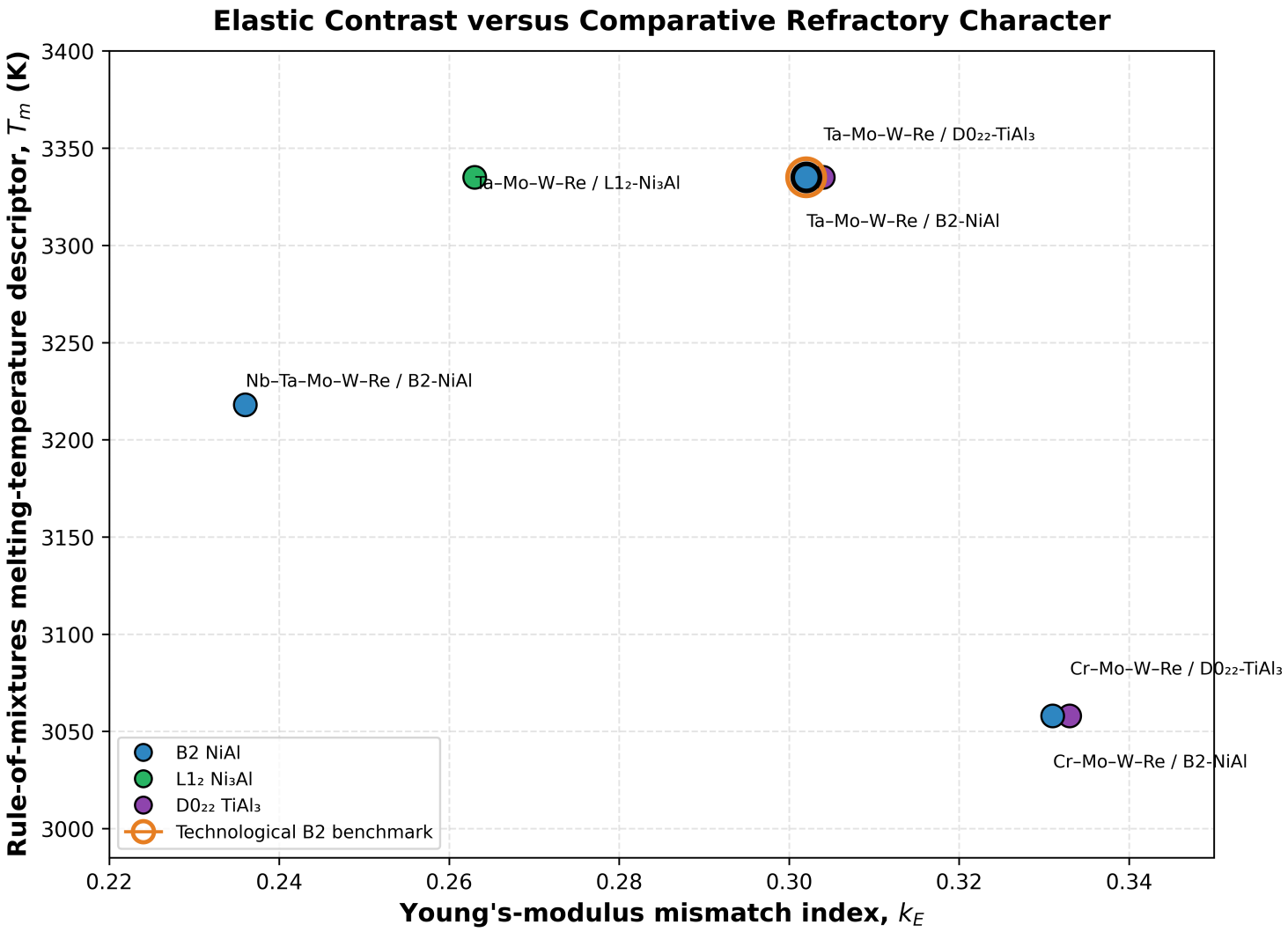


Figure 2

Elastic contrast versus comparative refractory character for the primary reference candidates. K_E is plotted against the rule-of-mixtures melting-temperature descriptor T_M. Ta–Mo–W–Re/B2-NiAl combines K_E = 0.302 with T_M = 3335 K. The map is not a phase-stability, liquidus-temperature, or service-performance diagram.

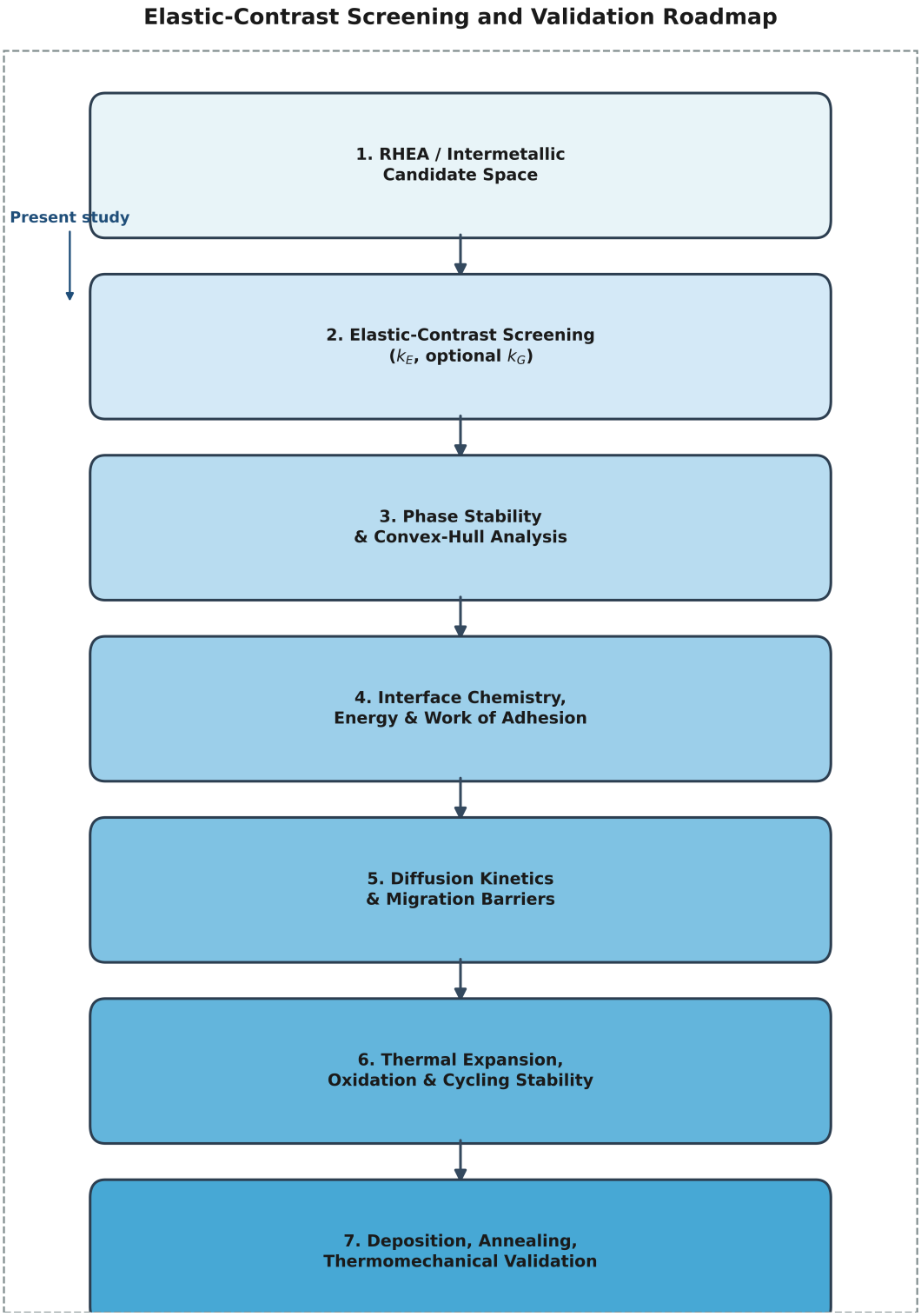


Figure 3

Elastic-contrast screening and validation roadmap for RHEA/intermetallic heterostructures. The workflow progresses from candidate-space definition and first-pass screening using K_E, and where available, K_G, through thermodynamic phase stability, interface chemistry and adhesion, diffusion, environmental stability, and experimental validation.